Scientific Research Publishing

Journal of Flow Control, Measurement & Visualization, 2022, 10, 76-85
https://www.scirp.org/journal/jfcmv
ISSN Online: 2329-3330
ISSN Print: 2329-3322

Trajectory Analysis of Particle Motions in Superfluid Helium-4 Using PTV Method

Lizhu Chen, Yoshiyuki Tsuji*

Department of Energy Engineering and Science, Nagoya University, Nagoya, Japan
Email: chen.lizhu@i.mbox.nagoya-u.ac.jp, *c42406a@nucc.cc.nagoya-u.ac.jp

How to cite this paper: Chen, L.Z. and Tsuji, Y. (2022) Trajectory Analysis of Particle Motions in Superfluid Helium-4 Using PTV Method. *Journal of Flow Control, Measurement & Visualization*, **10**, 76-85.
https://doi.org/10.4236/jfcmv.2022.102005

Received: December 22, 2021
Accepted: March 16, 2022
Published: April 27, 2022

Abstract

This paper describes the use of particle tracking velocimetry to analyze the Lagrangian acceleration of small particles in superfluid helium with varying time increments, Δt. The probability density of acceleration exhibits Gaussian properties for $\Delta t < \tau_0$, but displays a lognormal distribution for $\tau_0 < \Delta t$, where τ_0 is the migration time characterizing the particle motion. The particle trajectories are well characterized by the Hurst exponent H. For smaller time scales than τ_0, the trajectories exhibit linear motion ($H \simeq 1$), but have certain fractal properties with $H \simeq 0.6$ for time scales larger than τ_0.

Keywords

Superfluid, He II, Counterflow, Particle Tracking Velocimetry

1. Introduction

In recent years, there has been great progress in the study of superfluid helium flow fields, especially in thermal counterflows. Liquid helium undergoes a phase change at a low temperature of 2.17 K and becomes superfluid. Superfluid helium can be understood as a mixture of superfluid and normal flow components. Helium turbulence is an interesting area of research that is important in terms of both basic science and applications because the superfluid component has no viscosity [1]. In recent years, thermal countercurrent experimental systems have been used to conduct research on ^{4}He using solid hydrogen for the visualization of tracer particles [2]-[7]. Paoletti performed particle tracking velocimetry (PTV) analysis and calculated the probability density function (PDF) of the vertical velocity of the tracer particles, resulting in confirmation that the theoretical velocity of the normal flow component is almost the same as the experimental velocity [2]. Mantia *et al.* [6] pointed out that the PDFs of velocity and acceleration

have different shapes depending on the length scale, ℓ_{exp}, which may be the experimental probe length or the distance between the particles along the trajectories. The PDF shape exhibits an unclassical power-law tail for small ℓ_{exp}, but attains a classical Gaussian form as the length scale increases. In addition, the PDF tails of the horizontal acceleration approach a scale of $a^{-5/3}$ as the length scales decrease. Mastracci and Guo [7] developed a separation scheme for visualized particle motions in relation to quantum vortices, while Sakai *et al.* characterized the Lagrangian particle trajectories according to their curvature and acceleration [8]. Kubo *et al.* found that the tracer particle velocity and acceleration PDFs are highly dependent on the particle diameters. In addition, the Hurst exponent H, defined as $\left\langle \left| x(t+\tau)-x(t) \right|^2 \right\rangle = C\tau^{2H}$, where $x(t)$ is the particle position at time t and τ is the time lag, was used to characterize the particle trajectories. The Hurst exponent H significantly depends on the particle size and the time lag τ [9] [10]. However, the particle trajectories of the normal fluid have not been distinguished from those trapped by the superfluid (or quantum vortices). Therefore, in this study, the Lagrange trajectories are classified into two categories. One is the motion carried by the normal fluid and the other is that carried by the superfluid flow. The acceleration of particle motions in relation to the migration time of the Hurst exponent is also analyzed.

2. Experimental Condition

A stainless-steel cryostat with three visualization windows was used in the experiments. **Figure 1** shows a schematic of the cryostat. A rectangular channel (cross-section 20 × 20 mm^2 and height 260 mm) made of acrylic resin was positioned inside. The bath temperature T_B was set to 1.9 or 2.0 K. The plate heater was placed at the bottom of the channel, and the heat flux q was set to 800 W/m^2.

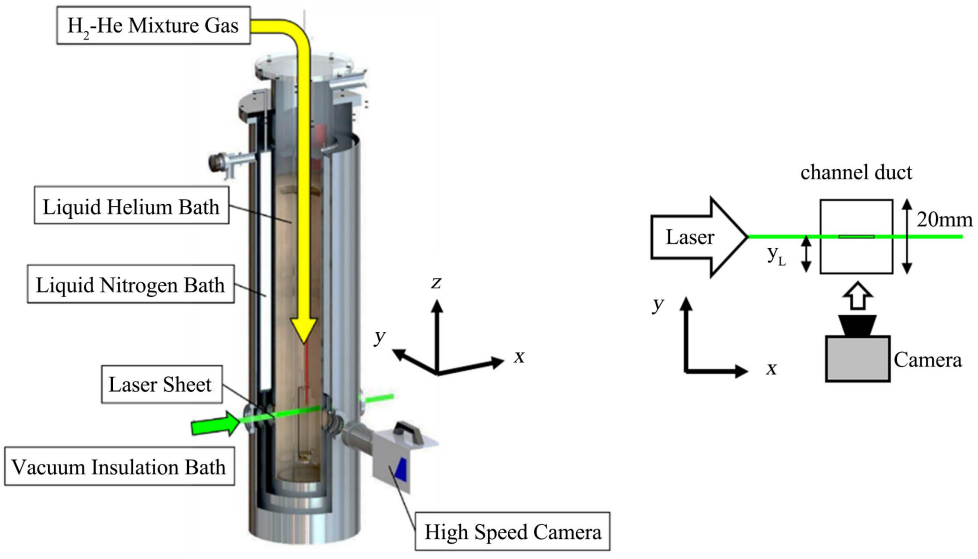

Figure 1. Schematic diagram of stainless steel cryostat.

A thermal counterflow was then generated inside the duct. The bath temperature was controlled by depressurizing the liquid helium layer along the saturation vapor pressure curve. A high-speed camera was used to visualize an area of 8.7×8.7 mm^2 at the duct center. The images were sampled at 250 Hz. A continuous laser was used to generate a laser sheet with a thickness of about 1 mm. The wall surface of the channel duct is defined as $y_L = 0$ mm and the center surface of the channel duct is defined as $y_L = 10$ mm. The visualization was performed at the center of the channel duct. The distance from the duct inlet to the visualization area was fixed at 93 mm to minimize the influence of disturbances. The experimental conditions are listed in Table 1.

A helium and hydrogen mixing chamber was designed to change the mixing ratio and spouting pressure. The hydrogen particles were generated in liquid helium. We adopted a mixing ratio of $He/H_2 = 40:1$ and a spouting pressure of 20 kPa. The images were recorded 90 s after injection. In this study, the particle tracking algorithm developed by our group was used. The particle sizes, $5 \le d \le 150$ μm, were similar to those in our previous experiments [9]. From the original image processing algorithm, the particle sizes were obtained by approximating the area S of a particle in two dimensions as a circle, whereupon the particle diameter d can be defined as $d = 2\sqrt{S/\pi}$ by further considering the effect of the Airy disk. Previously, we found that the particle size distribution can be accurately represented by a lognormal distribution and that smaller particles have better traceability [9] [10].

3. Statistical Analysis Method

We adopt the PTV algorithm to analyze the particle trajectories. In the first process, the background noise is removed to identify the particles. The position of each particle is then determined successively. It is very important to identify pairs of particles in consecutive images, as this affects the accuracy of the trajectory and velocity data. Previous studies typically considered the distance between a particle at successive time steps to be less than the distance to other particles [9]. As thermal convection has two components that move in opposite directions, using the distance of movement as a measure may misjudge the particle positions. We, therefore, identify individual particles by focusing on both the position and the particle size. Calibration was performed carefully through free-fall experiments to calculate the particle sizes. Particles with known diameters were visualized, and the freefall velocity was calculated from the visualization and compared with the terminal velocity [9].

Table 1. Experimental conditions for the current study.

Bath temperature (K)	Heat flux (W/m^2)	v_s (mm/s)	v_n (mm/s)
$T_B = 1.9$	800	−3.00	4.00
$T_B = 2.0$	800	−3.60	2.80

4. Results and Discussion

4.1. Particle Size Distribution and Its Classification

We analyzed the distribution of particle size d and found that the small hydrogen particles injected into the helium could be well approximated by the log-normal distribution [9]. The particle velocity depends on the particle size. A typical example of velocity distribution is shown in **Figure 2**. This shows the vertical component measured at the center of the duct with a bath temperature of $T_B = 1.9$ K and heat flux of $q \cong 800$ W/m^2. Negative and positive velocities correspond to downward particles trapped by a quantum vortex and upward particles carried by Stokes drag, respectively. To explore the effect of particle size on velocity, we calculated the velocity PDFs of different particle sizes and classified them into three groups. The PDF shape does not change when the particle diameter is less than 15 μm. These small particles are classified as S-size ($5 \le d \le 15$ μm); particles smaller than 5 μm could not be well identified because of the spatial resolution. A bimodal velocity distribution can be observed for particles in the range $15 \le d \le 25$ μm, which are classified as M-size. Larger particles with $25 \le d \le 150$ μm, classified as L-size, exhibit a single-peak velocity distribution. The S- and M-size particles have obvious bimodal distributions. The right peak corresponds to upward particle velocities, in the same direction as the heat flow. These particles are entrained by the viscous normal fluid flow. The peak on the left corresponds to the downward velocity, *i.e.*, particles moving in the opposite direction to the heat flux. Particles trapped by the local minimum pressure core of quantum vortices are carried in the downward direction. The L-size particles are less dependent on the background flow. They have a mean positive velocity and follow the normal fluid motion.

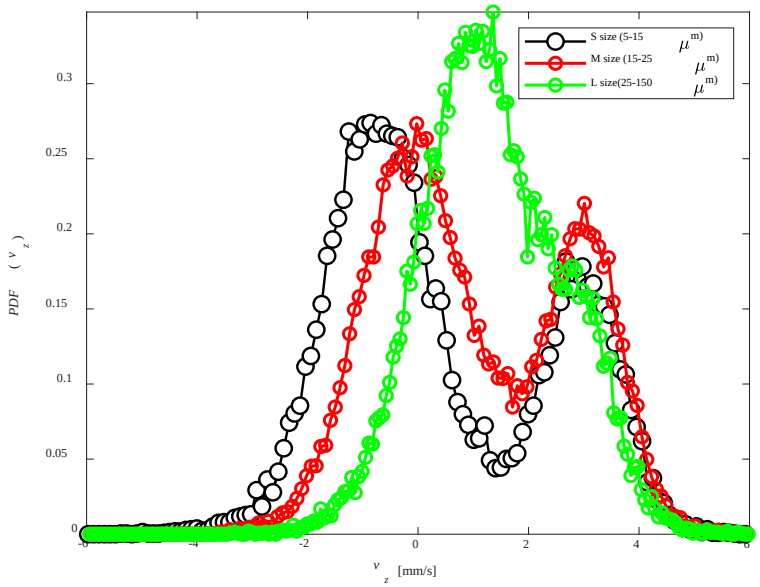

Figure 2. Vertical velocity probability density functions. The bath temperature is $T_B = 1.9$ K and heat flax is $q \cong 800$ W/m^2.

According to the two-fluid model [1], the mean velocity of particles entrained by the viscous normal fluid is $v_n = q/\rho s T_B$, where q is the heat flux, ρ is the He II density, and s is the He II specific entropy. The velocity in the downward direction is given by $v_s = v_n \rho_n / \rho_s$, where ρ_n / ρ_s is the density ratio of the two fluids. Particles trapped by the local minimum pressure core of quantum vortices are carried in the downward direction.

4.2. Particle Trajectories

To further study the specific manifestations of Lagrangian particle trajectories, we refer to a previous method for distinguishing between particles that follow the normal and superfluid compositions [7]. By considering Gaussian fits to the bimodal distributions, we obtain their respective mean velocities ($\overline{v}_1$ and $\overline{v}_2$) and standard deviations (σ_1 and σ_2). As the left and right peaks are clearly distinguishable in the present research and the relative speed is low, the condition $\overline{v}_1 + \overline{v}_2 > \sigma_1 + \sigma_2$ always holds. The vertical mean velocity was calculated for each particle trajectory, and is expressed as $\overline{v}_z$ hereafter. For each particle trajectory, if $\overline{v}_z < \overline{v}_1 + \sigma_1$ holds, the particle is categorized as a superfluid particle. Otherwise, if $\overline{v}_z > \overline{v}_2 - \sigma_2$, the particle is treated as a normal fluid particle trajectory. If the mean vertical velocity $\overline{v}_z$ is in the range $\overline{v}_1 + \sigma_1 \le \overline{v}_z \le \overline{v}_2 - \sigma_2$, the trajectory is neglected in this study, because these trajectories cannot be clearly classified as either superfluid or normal fluid motion.

The trajectory for each particle size is shown in **Figure 3**. The red lines are the trajectories of tracer particles following the normal fluid component. As the normal fluid maintains a laminar flow state in the current heat flux range, the trajectories are relatively straight. The blue lines are the trajectories of tracer

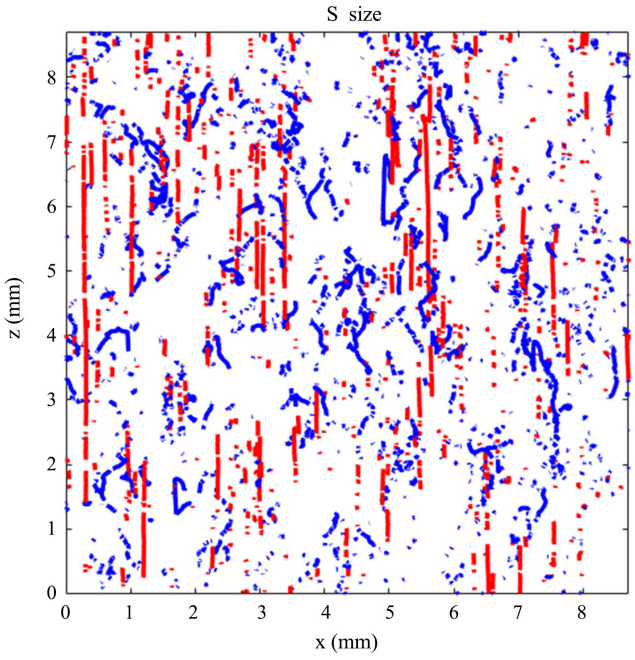

(a)

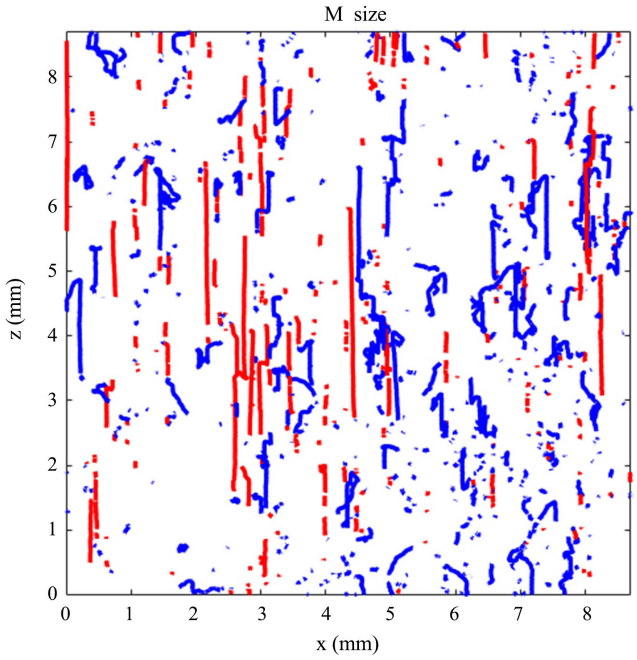

(b)

Figure 3. Trajectory diagram of particles: (a) S-size; (b) M-size. The bath temperature is $T_B = 1.9$ K and heat flax is $q \cong 800$ W/m^2.

particles following the superfluid component. Such particles are trapped by vortices, resulting in irregular trajectories. In addition, due to the three-dimensional motion of the quantum vortices, it is difficult for the particles to remain in one plane for a long time, so the blue trajectories are relatively short.

4.3. Hurst Exponent

In our previous research [9] [10], the Hurst exponent H was calculated as $\overline{\left|z(t+\tau)-z(t)\right|^2} = C\tau^{2H}$, where $z(t)$ is the vertical component of the particle position at time t and τ is the time lag. An example is shown in **Figure 4**. For small values of the time lag, the exponent is $H_1 \simeq 1$ and the trajectory can be approximated by linear motion. For larger time lags as $\tau_0 \le \tau$, the exponent is $H_2 \simeq 0.6$ and the trajectory displays a fractal property. The inset shows the normalization $\overline{\left|z(t+\tau)-z(t)\right|^2} / C\tau^{2H_1}$. Therefore, the migration time scale τ_0 characterizes the transition from linear to fractal self-similar particle motions.

These particle motions have interesting acceleration statistics. In the next subsection, we present the particle acceleration calculated at different time scales.

4.4. Probability Density Function of Vertical Acceleration

The particle acceleration was analyzed for the three different particle sizes within the normal and superfluid components. Among these, the S-size particles within the superfluid component are the focus of this subsection because of the clear

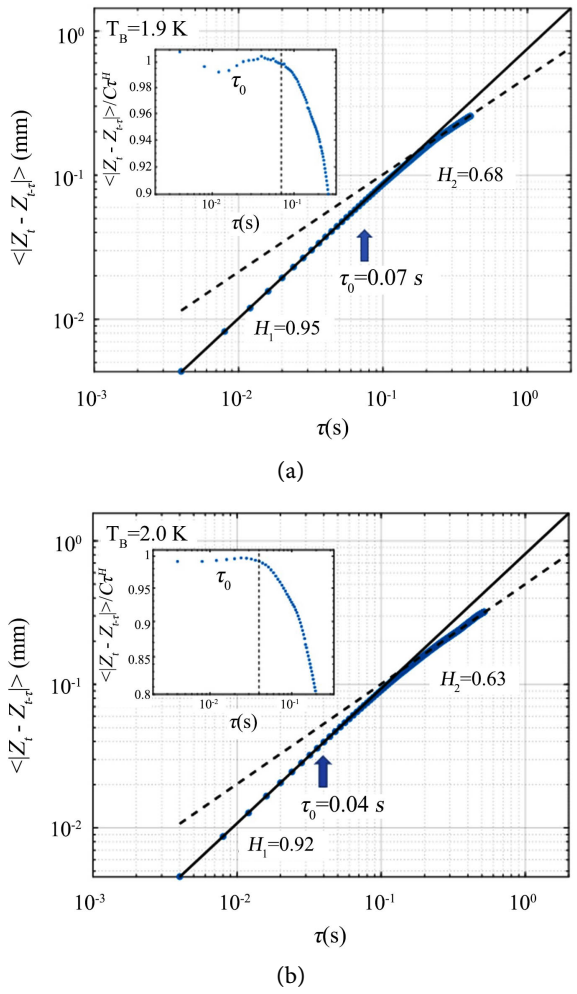

Figure 4. Relation between vertical increment and time lag. (a) $T_B = 1.9$ K and heat flux is $q \cong 800$ W/m^2; (b) $T_B = 2.0$ K and heat flux is $q \cong 800$ W/m^2.

interaction with quantum vortices. The acceleration was calculated using the second-order central differential formula. The time increment Δt used to calculate the differential was set to several different values. We are interested in the cases $\Delta t < \tau_0$ and $\tau_0 < \Delta t$. With a small time increment ($\Delta t < \tau_0$), the acceleration PDF can be accurately approximated by a general Gaussian distribution. A typical example of vertical acceleration with a bath temperature of $T_B = 1.9$ K and heat flux of $q \cong 800$ W/m^2 is shown in **Figure 5**. However, for large time increments ($\tau_0 < \Delta t$), the tail of the PDF deviates from a Gaussian distribution. Such a trend has been observed in quantum fluid turbulence. The tail can be approximated by the following lognormal distribution, where s is the intermittency exponent:

$$p(\alpha) = \frac{1}{4\sqrt{3}} \exp\left(\frac{3s^2}{2}\right)\left[1 - \operatorname{erf}\left(\frac{\ln\left|\alpha/\sqrt{3}\right| + 2s^2}{\sqrt{2}s}\right)\right] \quad (1)$$

Mantia *et al.* suggested $s = 1$ to represent the tail part when the time lag is

smaller than the integral scale [6]. For smaller time lags, however, a power-law distribution is better than a lognormal distribution in terms of approximating the tail part. In our analysis, $s=1$ is good, but not sufficient to represent the tail part. This may be because high-acceleration events occur more frequently when the particle trajectory has fractal geometry features. The PDFs analyzed in the time increment $\tau_0 < \Delta t$ collapse sufficiently well as shown in **Figure 6**. Therefore, the PDFs are self-similar in these time scales. For smaller time increments, $\Delta t < \tau_0$, the PDFs are close to Gaussian. This is contrary to the previous result, but may be caused by high-acceleration events such as vortex reconnections being neglected in our trajectory-identification algorithm. We are analyzing Lagrangian trajectories as far as the particles are tracked and carried by quantum vortices. Once vortex reconnection occurs, the particle position changes significantly, but particle tracking stops at that point.

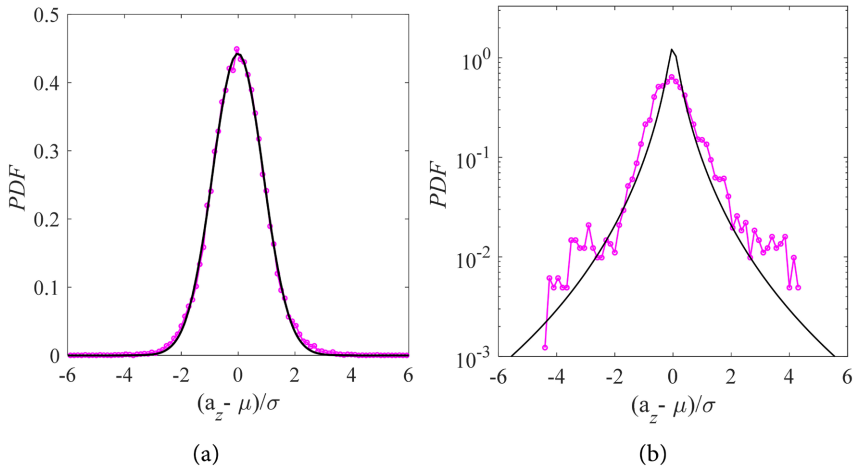

Figure 5. PDF of vertical acceleration at $T_B = 1.9$ K and heat flux of $q \cong 800$ W/m^2. (a) $\Delta t/\tau_0 = 0.06$ and solid line is a general Gaussian distribution, (b) $\Delta t/\tau_0 = 1.50$ and solid line is a lognormal distribution with $s=1$.

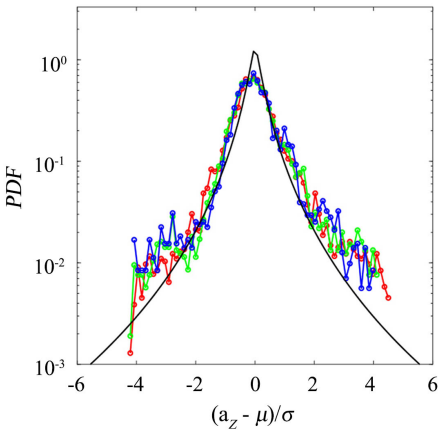

Figure 6. PDF of vertical acceleration at $T_B = 1.9$ K and heat flux of $q \cong 800$ W/m^2. Red solid circles are $\Delta t/\tau_0 = 1.0$, green solid circles are $\Delta t/\tau_0 = 1.5$, and blue solid circles are $\Delta t/\tau_0 = 2.0$. Solid line is lognormal distribution with $s=1$.

As shown in Figure 3, the downward particle trajectories are complicated. Small particles trapped by quantum vortices are carried downward while interacting with other vortices or tangles. Lagrangian acceleration was analyzed along such trajectories.

5. Conclusion

We have classified the particle sizes into three groups (S-, M-, and L-size) and analyzed the Lagrangian trajectories and their acceleration. The particle motions were divided into superfluid and normal fluid components depending on their velocity PDFs. The features of S-size particles within the superfluid component interacting with quantum vortices were studied, and the results can be summarized as follows. 1) The velocity distribution is affected by the particle size. Particles smaller than 15 μm may be trapped by quantum vortices. 2) Particle acceleration exhibits a general Gaussian distribution for time increments of $\Delta t < \tau_0$, but can be better approximated by a lognormal distribution for $\tau_0 < \Delta t$. Here, τ_0 is the migration time scale for characterizing the transition from linear to fractal self-similar particle motions. 3) The acceleration PDFs normalized by the mean and standard deviation exhibit shape-invariance for $\tau_0 < \Delta t$. That is, their PDFs have self-similar shapes as far as the particle trajectories display inherent fractal properties.

Acknowledgements

We are grateful to Mr. Maruyama for his help in measuring the experimental data. This work was partly supported by JSPS KAKENHI through Grant Numbers JP19H00641 and JP19H00747.

Conflicts of Interest

The authors declare no conflicts of interest regarding the publication of this paper.

References

[1] Landau, L. (1941) Theory of the Superfluidity of Helium II. *Physical Review*, **60**, 356-358. https://doi.org/10.1103/PhysRev.60.356

[2] Paoletti, M.S., Florlto, R.B., Sreenivasan, K.R. and Lathrop, D.P.J. (2008) Visualization of Superfluid Helium Flow. *Journal of the Physical Society of Japan*, **77**, Article ID: 111007. https://doi.org/10.1143/JPSJ.77.111007

[3] Bewley, G.P., Lathrop, D.P. and Sreenivasan, K.R. (2006) Visualization of Quantized Vortices. *Nature*, **441**, Article No. 588. https://doi.org/10.1038/441588a

[4] Murakami, M., Takakoshi, T., Maeda, M., Tsukahara, R. and Yokota, N. (2009) Application of Particle Image Velocimetry for Measuring He II Thermal Counterflow Jets. *Cryogenics*, **49**, 543-548. https://doi.org/10.1016/j.cryogenics.2008.10.020

[5] Chagovets, T.V. and Sciver, S.W. (2011) A Study of Thermal Counterflow Using Particle Tracking Velocimetry. *Physics of Fluids*, **23**, Article ID: 107102. https://doi.org/10.1063/1.3657084

[6] La Mantia, M. and Skrbek, L. (2014) Quantum Turbulence Visualized by Particle Dynamics, *Physical Review B*, **90**, Article ID: 014519. https://doi.org/10.1103/PhysRevB.90.014519

[7] Mastracci, B. and Guo, W. (2018) Exploration of Thermal Counterflow in He II Using Particle Tracking Velocimetry. *Physical Review Fluids*, **3**, Article ID: 063304. https://doi.org/10.1103/PhysRevFluids.3.063304

[8] Sakaki, N., Maruyama, T. and Tsuji, Y. (2022) Statistics of the Lagrangian Trajectories' Curvature in Thermal counterflow. *Journal of Low Temperature Physics*, in press. https://doi.org/10.1007/s10909-022-02674-3

[9] Kubo, W. and Tsuji, Y. (2019) Statistical Properties of Small Particle Trajectories in a Fully Developed Turbulent State in He-II. *Journal of Low Temperature Physics*, **196**, 170-176. https://doi.org/10.1007/s10909-019-02192-9

[10] Chen, L., Maruyama, T. and Tsuji, Y. (2022) Statistical Property of Lagrangian Trajectory of Small Particles in Super Fluid He4. *Journal of Low Temperature Physics*, in press. https://doi.org/10.1007/s10909-022-02691-2